

EFFECT OF INTER-LAYER COOLING TIME ON DISTORTION AND MECHANICAL PROPERTIES IN METAL ADDITIVE MANUFACTURING

Y.K. Bandari*, Y.S. Lee, P. Nandwana, B.S. Richardson, A.I. Adediran, L.J. Love

*Manufacturing Demonstration Facility, Oak Ridge National Laboratory, Knoxville, TN, 37932,
USA

Abstract

Laser Metal Deposition with wire (LMD-w) is one of the novel Direct Energy Deposition (DED) processes that is gaining the attention of various industries, especially aerospace, due to the potential cost and lead time reductions for complex parts. However, subjects of development include optimization of process parameters (for example laser power, wire feed speed, robotic travel speed, inter-layer cooling time etc.) for large scale adaption of this process. These parameters influence residual stress which potentially results in distortion and subsequent mechanical properties. Inter-layer cooling time is one of the main influences on production volume and is typically used to help control the cooling conditions to mitigate part distortion. Therefore, this paper is aimed at investigating different inter-layer cooling times on distortion and resulting mechanical properties of the parts produced by LMD-w. Distortion of deposited Ti-6Al-4V walls was measured automatically using a laser scanner, which was attached to the robotic arm itself. Finally, suitable recommendations are discussed to optimize the inter-layer cooling time to produce parts with desired mechanical properties.

Keywords: Additive Layered Manufacturing, 3-D Printing, Direct Energy Deposition, Laser Metal Deposition with wire, Ti-6Al-4V, Laser Scanner, Distortion, Residual Stress

1. Introduction

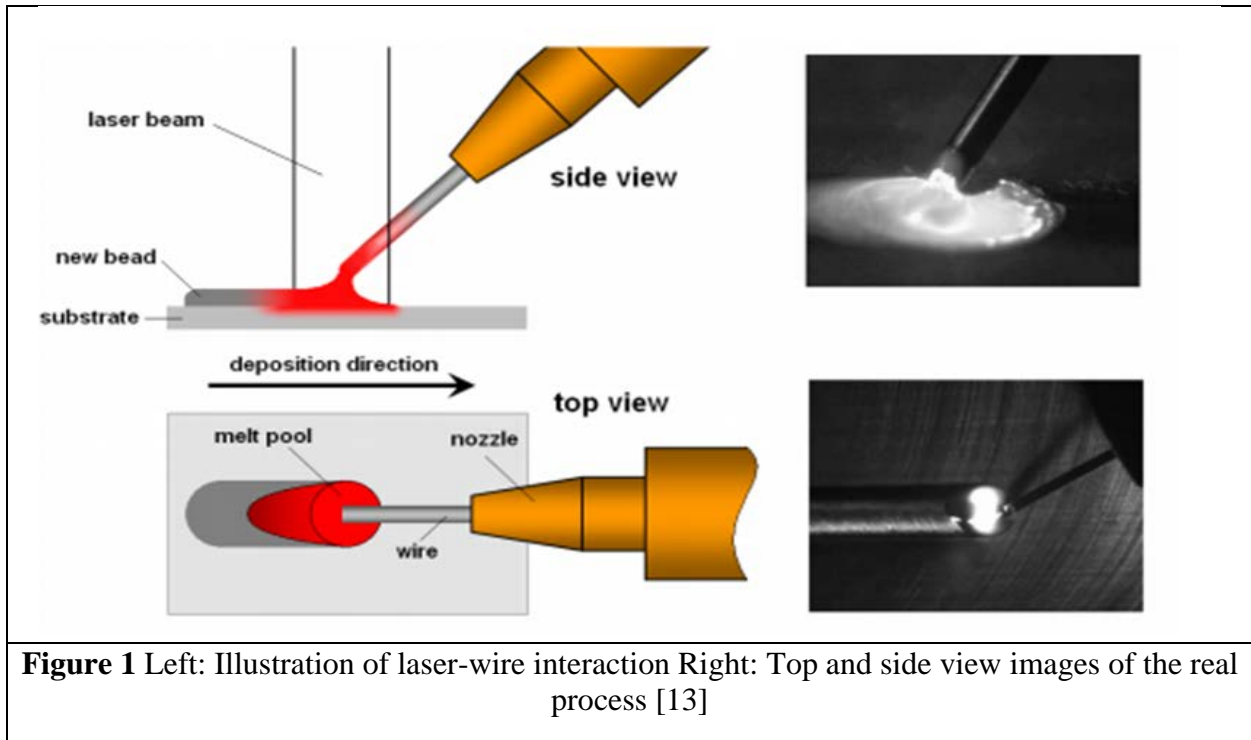
Since their first introduction more than 30 years prior, additive manufacturing (AM) processes for metals have been produced and commercialized in the market under different names, for example, Direct Metal Deposition [1], Laser Engineered Net Shaping [2], Shaped Metal Deposition [3], Selective Laser Melting [4], and Electron Beam Freeform Fabrication [5]. In every one of these processes, a heat source is used to create a melt pool into which a wire or powderized feedstock is fed, or the heat source is applied to a powder bed to create beads after solidification. The beads are realized by relative movement of the melt pool and the substrate by using an industrial robotic arm or a gantry system [6]. A part is then manufactured by depositing beads adjacent to each other and layer upon layer. The most common technique to date has been to use a high-power laser as the heat source with metal powder as the feed stock. Other conventional welding techniques have likewise been introduced, for example, Tungsten Inert Gas (TIG) welding [7], Gas Metal Arc Welding (GMAW) [8], Plasma Transferred Arc (PTA) welding [9], [10], and Electron Beam (EB) welding [11].

The high-power laser-based technique remains the most common because of several advantages, for example, the relatively low heat input to the base material and good shape accuracy of the realized geometries. This Laser Metal Deposition (LMD) process has been dominated by

Notice of Copyright. This manuscript has been authored by UT-Battelle, LLC under Contract No. DE-AC05-00OR22725 with the U.S. Department of Energy. The United States Government retains and the publisher, by accepting the article for publication, acknowledges that the United States Government retains a non-exclusive, paid-up, irrevocable, world-wide license to publish or reproduce the published form of this manuscript, or allow others to do so, for United States Government purposes. The Department of Energy will provide public access to these results of federally sponsored research in accordance with the DOE Public Access Plan (<http://energy.gov/downloads/doe-public-access-plan>).

powder-based technologies because of flexibility and robustness of the process. However, the powder-based technologies have been developed for building small and complex geometries, with very little focus on deposition rate. The deposition efficiency varies depending on the system set-up, and post treatment of the scattered powder is required. For large scale parts with moderate complexity, such as flanges or bosses, it is more rewarding to use wire-based processes, since these lead to higher deposition rates, better material quality and better surface finish [12]. While the utilization of powder requires specially planned and designed feeding nozzles, the wire-based processes require much simpler equipment and standard welding hardware.

Laser Metal Deposition with wire (LMD-w) is a novel process that fabricates components using a high-power laser source and adds material in the form of metal wire. The laser generates a melt pool on the substrate material into which the metal wire is fed and melted, forming a metallurgical bond with the substrate [13]. By moving the laser processing head and the wire feeder, i.e. the welding tool, relative to the substrate a weld bead is formed during solidification. The relative movement of the welding tool and the substrate is made using a 6-axis industrial robot arm. The formation of a weld bead is illustrated in Figure 1 along with images from the real process.



One main consideration for the resulting parts of the LMD-w process is the dimensional precision compared to an initial input geometry. Each layer is formed by melting individual passes from the wire, which experiences rapid heating, melting, solidification, and cooling during the deposition process. While the part is manufactured, the deposited material experiences continuous heating and cooling cycles as more passes and layers are deposited. One of the consequences of the thermal gradients induced in the components by the layer-by-layer deposition of material in AM processes is the build-up of undesirable levels of residual stress and distortion [14].

2. Literature Review

The development of residual stress and distortion in AM processes has several similarities with multi-pass welding. Several researchers have explored techniques to reduce distortion in similar multi-pass welding processes including the investigations by Michaleris and DeBiccari [15] who demonstrated that decreasing heat input would result in a decrease in workpiece distortion and Masubuchi [16] who confirmed that constraining the workpiece can limit distortion. Furthermore, Deo and Michaleris [17] examined the impact of heating the weld region immediately prior to welding and found that the technique can be utilized to achieve zero net distortion. In AM research Klingbeil et al. [18] and Cornin et al. [19] each found that bulk substrate preheating can be used to decrease distortion in deposited workpieces.

In AM processes, the influence of change in path planning and inter-layer cooling time between passes on residual stress and distortion have also been studied. For instance, the selection of different deposition paths has been shown by Nickel et al. [20] to notably affect distortion in AISI 1117 C-Mn steel, and has also been studied by Mercelis and Kruth (2001) to influence residual stress in AISI 316 austenitic stainless steel. With respect to changing inter-layer cooling time between passes, Jendrzewski et al. (2007) reported that shorter delays reduce the measured residual stress in deposited Cobased stellite SF6 alloy, and Klingbeil et al. [18] concluded delays to reduce distortion in AISI 308 austenitic stainless steel. Fessler et al. [21] reported that allowing deposition to cool between passes decreases distortion of nickel-base INVAR alloys and austenitic stainless steels. Costa et al. [22] and Torries et al. [23] studied the effect of introducing inter-layer cooling time between deposited layers on the resulting thermal history and microstructure of laser deposited AISI 420 steel and Ti-6AL-4V respectively. The study concluded that low inter-layer cooling times result in higher temperature levels and notably altered microstructure when compared with longer inter-layer cooling times.

Whereas these studies have concentrated on post-process measurements of accumulated distortion, others have used in-situ measurements to monitor the temporal accumulation of distortion. Lundbäck [24] estimated in-situ distortion on single wall builds utilizing an optical measurement system to validate their model of the GTAW process. Plati et al. [25] utilized a linear variable differential transformer to measure the deflection of the free end of a cantilevered substrate during powder-based cladding. Grum et al. [26] recorded in-process strain using resistance measuring rosettes to measure strain accumulation during laser cladding. Ocelik et al. [27] utilized digital image correlation to measure distortion of single and multi-bead Nanosteel, Eutroloy 16012, and MicroMelt 23 powder laser depositions on C45 steel and 301 stainless steel substrates. The in-situ measurements taken in these works offer more prominent understanding into distortion accumulation than conventional post-process distortion measurements, but do not compare the impact of changing materials or inter-layer cooling time. The in-situ distortion measurements have primarily been conducted for model validation. Also, some of the other researchers Ding et al. [28], [29], [30], Montevecchi et al. [31], Simunovic et al. [32] have developed thermo-mechanical models to predict residual stress and the resultant distortion in the large parts. However, the relationship between inter-layer cooling time and heat input was not discussed and then interlayer cooling time is one of the parameters which affects the overall production rate.

Much of this previous work on the accumulation of distortion during the deposition has focused on welding and laser cladding processes. AM, on the other hand, involves the deposition of

multiple layers and potentially large volumes of material to produce discrete shapes and components. In cases where AM processes have been investigated, the impact of changes in the inter-layer cooling time between multiple passes on the accumulation of distortion and the impact on the mechanical properties of the realized components has not been investigated. In the work reported here, in-situ measurements of distortion during the deposition of Ti-6Al-4V are made to investigate the effect of inter-layer cooling time on the mechanical properties.

3. Experimental Procedure

This section describes the base materials, consumables, deposition conditions, power supplies, set-up and techniques deployed during the investigation. The experiments were performed using Ti-6Al-4V plates and delivered according to the specifications AMS 4911; a 1.6 mm diameter Ti-6Al-4V solid wire consumable was used and delivered according to the specifications AMS 4954. The compositions in wt.% for substrate and electrode wire are shown in the Table 1.

Table 1 Chemical composition of substrate and wire

| Element | Substrate (wt.%) | Wire (wt.%) |
|----------------|------------------|-------------|
| Carbon | 0.01 | 0.02 |
| Iron | 0.16 | 0.18 |
| Aluminum | 6.35 | 6.03 |
| Titanium | Remainder | Remainder |
| Vanadium | 4.13 | 4.08 |
| Hydrogen (ppm) | 25 | 25 |
| Nitrogen | 0.01 | 0.01 |
| Oxygen | 0.19 | 0.18 |

3.1 Preparation of substrate

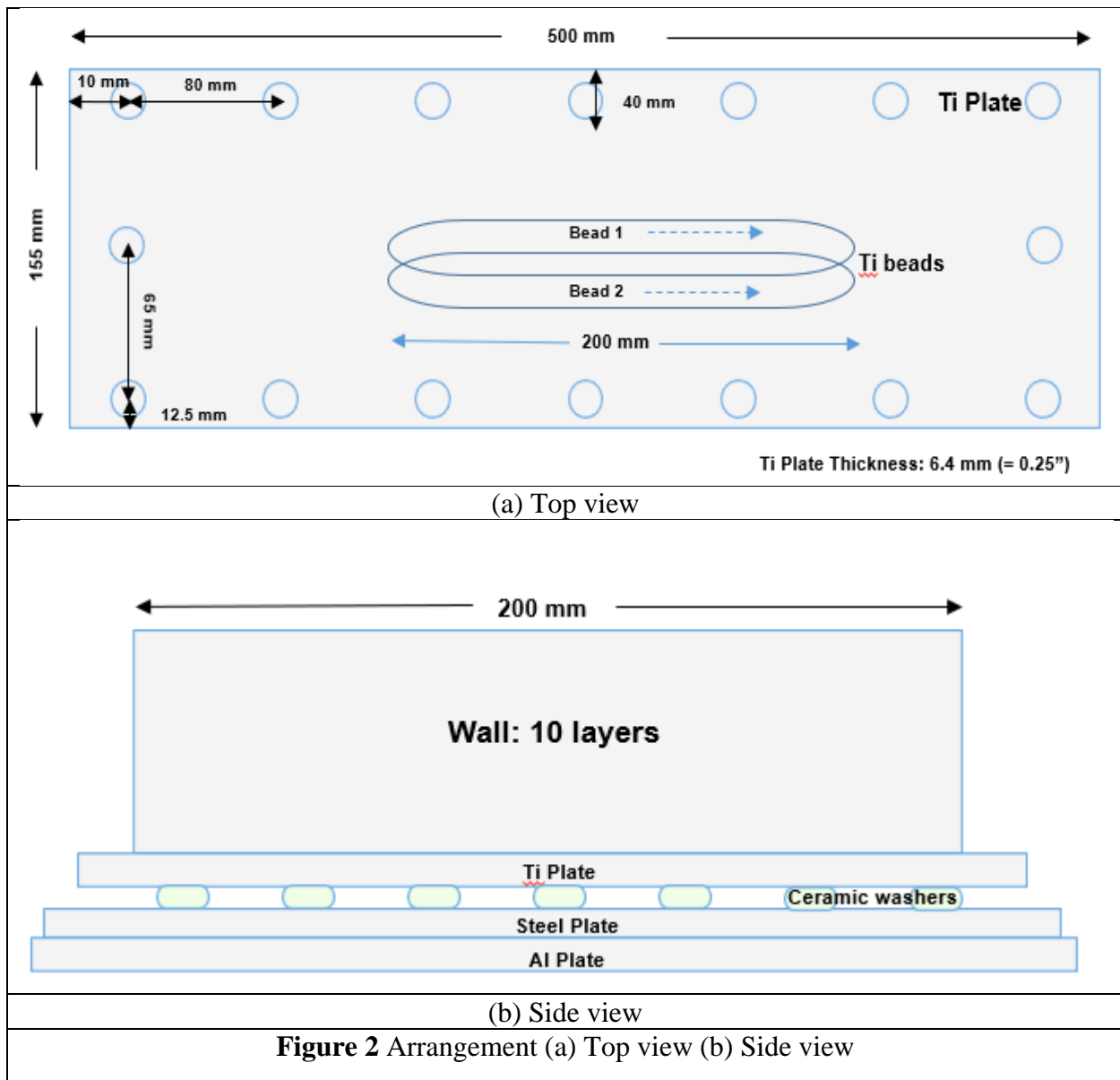
The titanium substrates were cut from a large titanium plate with a thickness of 6.4 mm. The dimensions of the substrate used for the investigation was 500 mm x 155 mm. The substrate's surface was first wiped using an acetone dampened clean paper cloth. Then a finishing disk Cibo SAG/5/115 was mounted on a hand-held grinder with a low rotational speed and the surface was ground to eliminate oxide layers and impurities. Finally, degreasing was repeated using the acetone dampened clean paper cloth. The substrate was clamped onto a steel block with ceramic washers in between them to avoid heat transfer through conduction. The steel block was then placed onto an aluminum table. A schematic diagram of the arrangement is shown in Figure 2.

3.2 Equipment set-up

All the investigations were conducted with a 6-axis KUKA 'KR90 2900 extra HA' robot. Two fiber delivered diode lasers each with the power of 10.7 kW and wavelengths of 940 – 980 nm and 1020 – 1060 nm were used, and they were combined using a laser head combiner to form a laser with 20 kW power. The laser light was conveyed to the optics to eventually form a 7.69 mm diameter out of focus laser spot on the work piece. Abicor Binzel was used as the wire feeder.

All the investigations were performed in a closed argon environment with less than 250 ppm O₂ content. The equipment set up is shown in Figure 3.

A laser line scanner was added to the system to measure the height of deposited layers, and it enabled the implementation of layer height control. It scans from the left end of the plate to the right end of the plate and records data for every 0.5 mm of travel. The laser scanner then generates layer height maps; subsequently, the correction data for the subsequent layer is generated from the control algorithm generated in-house, to maintain a set layer height for all the layers. The control algorithm was developed using LabVIEW™ software and was executed in a computer. LabVIEW™ software was also used to interface with the robot, laser and wire feed systems as well as collecting and logging data.



3.3 Design of Experiments

The weld parameters used for deposition are listed below in Table 2. The dimensions of the walls were $200 \times 20 \times 11 \text{ mm}^3$. Continuous weld beads 200 mm long were deposited one layer at a time in the same deposition direction. With the weld parameters listed below, the single bead width and single bead height ranged between $9\text{-}12 \text{ mm}$ and $0.8\text{-}1.2 \text{ mm}$ respectively. Thus, two beads were deposited next to each other with an overlap that resulted in a flat deposited layer of width 21 mm .

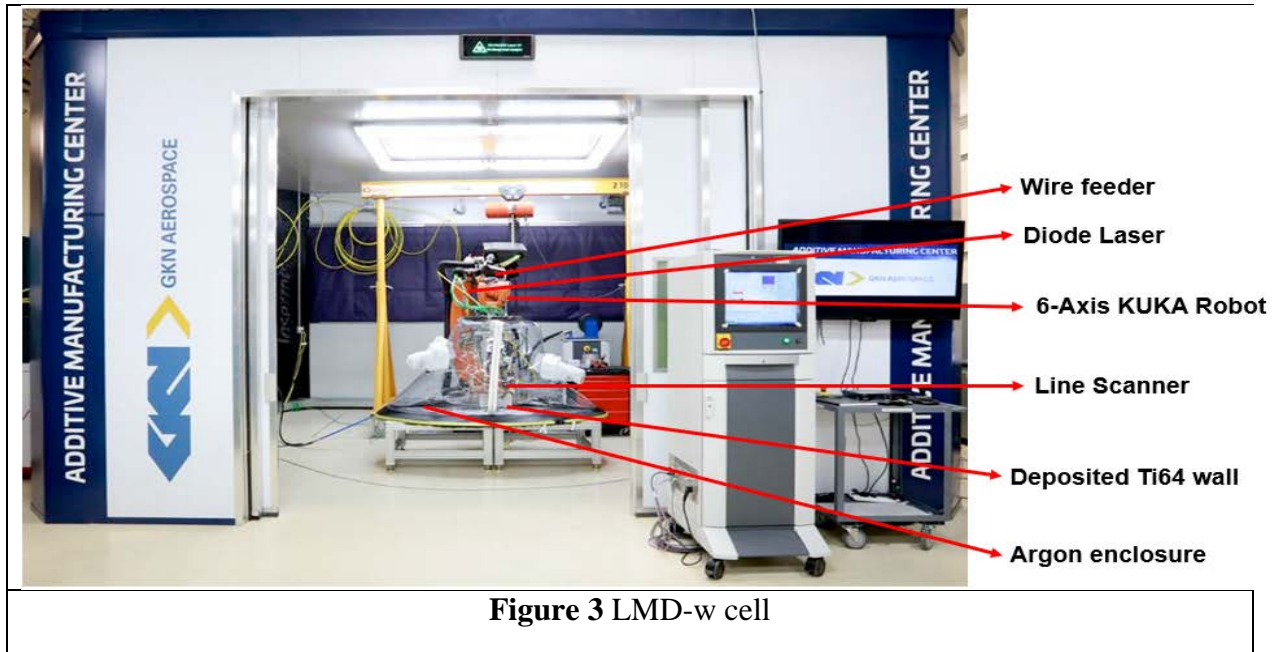


Figure 3 LMD-w cell

Table 2 Deposition and weld bead parameters

| Parameter | Value |
|--------------------|-------------------|
| Laser power | 11.5 kW |
| Robot travel speed | 12 – 14 mm/s |
| Deposition rate | 2.0 +/- 1.0 kg/hr |
| Single bead width | 9-12 mm |
| Single bead height | 0.8-1.2 mm |

Before depositing a new layer, the previously deposited layer was scanned using the laser line scanner, and the height data was recorded. To maintain a constant layer height, the control algorithm created new weld parameters which were then used to deposit the subsequent layer automatically. In total six walls were deposited. Three of them were clamped all-round the substrate, and three were clamped only at the center. Interlayer cooling time is the wait time between the end of depositing a layer and start of height scan for that layer. Each wall was deposited using a different interlayer cooling time. In total ten layers were deposited for each wall. The six walls are denoted as Wall 1, Wall 2 and so on until Wall 6 and are described below.

Wall 1 was built with clamps all-round the substrate with no inter-layer cooling time. Wall 2 was built with clamps all-round the substrate with an inter-layer cooling of 30 min after depositing every five layers. Wall 3 was built with a center clamp with no inter-layer cooling time. Wall 4 was built with clamps all-round the substrate with an inter-layer cooling time of 30 min after depositing every two layers. Wall 5 was built with center clamp with an inter-layer cooling time of 30 min after depositing every two layers. Wall 6 was built with center clamp with an inter-layer cooling time of 30 min after depositing every five layers. These are described in the form of a table below (Table 3).

Table 3 Description of walls deposited

| Sample | Clamped/unclamped | Inter-layer cooling time of 30 min after every 'n' layers of deposition (n) |
|--------|-------------------|---|
| Wall 1 | Clamped | 10 |
| Wall 2 | Clamped | 5 |
| Wall 3 | Unclamped | 10 |
| Wall 4 | Clamped | 2 |
| Wall 5 | Unclamped | 2 |
| Wal 6 | Unclamped | 5 |

4. Results and discussion

Below are the graphs that show a correlation between the layer number and vertical deformation for each wall. Figure 4 and Figure 5 show the vertical deformations of the plate at the left end and right end of the plate respectively with respect to the layer number.

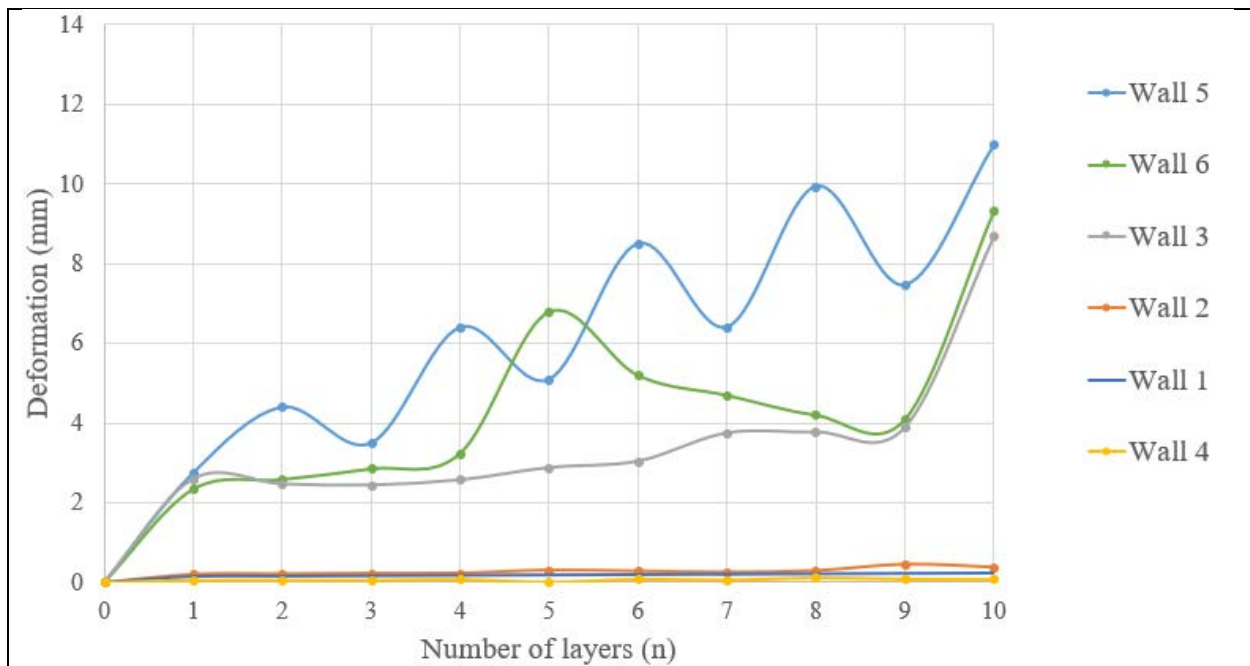


Figure 4 Deformation of left end of the plate with an increase in layer number

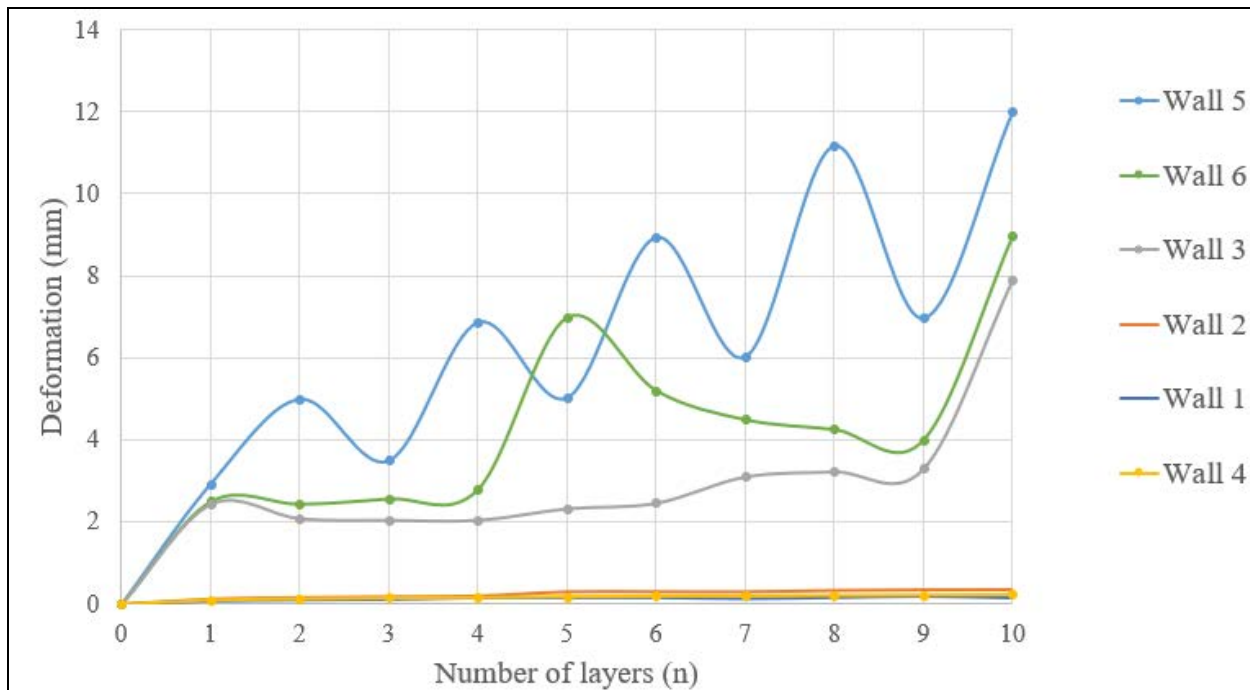


Figure 5 Deformation of right end of the plate with an increase in layer number

The vertical deformation on layer zero indicates the deformation of the plate without any deposited material. Likewise, the vertical deformation on layer 10 indicates the deformation of the plate after 10 layers of deposition and 30 min of cooling time.

As shown in Figure 4 and Figure 5, the walls built using only center clamps experienced more vertical deformation on the right end of the plate than on the left end of the plate; the vertical deformation also increased as more layers were deposited. This is due to the preheating effect. The robot moves from the left end to the right end of the plate depositing beads from left to the right. Therefore, the heat also transfers from left to right and downwards through conduction mode primarily. There is more heat accumulation on the right end compared to the left end, which is also seen from the thermocouple readings, that were attached on the both ends of the plate. Subsequently, there is more residual stresses and thus, more deformation. Therefore, the deformation at the right end of the plate is more than the deformation at the left end of the plate.

It is also seen that deformation increases with both an increase in layers and the introduction of inter-layer cooling time; the, deformation decreases after depositing the subsequent layer. From Figure 6, it is seen in the case of Wall 5, which was built using only center clamps and with an inter-layer cooling time after every two layers. The deformation before the third layer of deposition was 4.5 mm, and then it decreased to 3.5 mm just before fourth layer of deposition. A similar trend was seen for Wall 3 and Wall 6, too. This trend is due to the shrinkage of the deposited metal, which causes the plate edges to lift resulting in vertical deformation. Then when a subsequent layer is deposited after the inter-layer cooling time, the deposited metal adds heat to the previously deposited layers, which then expand and lower the edges of the plate [14].

In case of walls built with clamps all-round the substrate, the deformation was found to be nearly zero, both at the left and right ends of the plates irrespective of inter-layer cooling times.

After depositing 10 layers with inter-layer cooling time and allowing them to cool down, all the Ti-6Al-4V plates were un-clamped. Then, the distortion at the right end of the plate was measured. Figure 6 shows the distorted plates after un-clamping. The vertical deformation at the right end of the plate for each wall is measured using a ruler and is presented in Table 3.

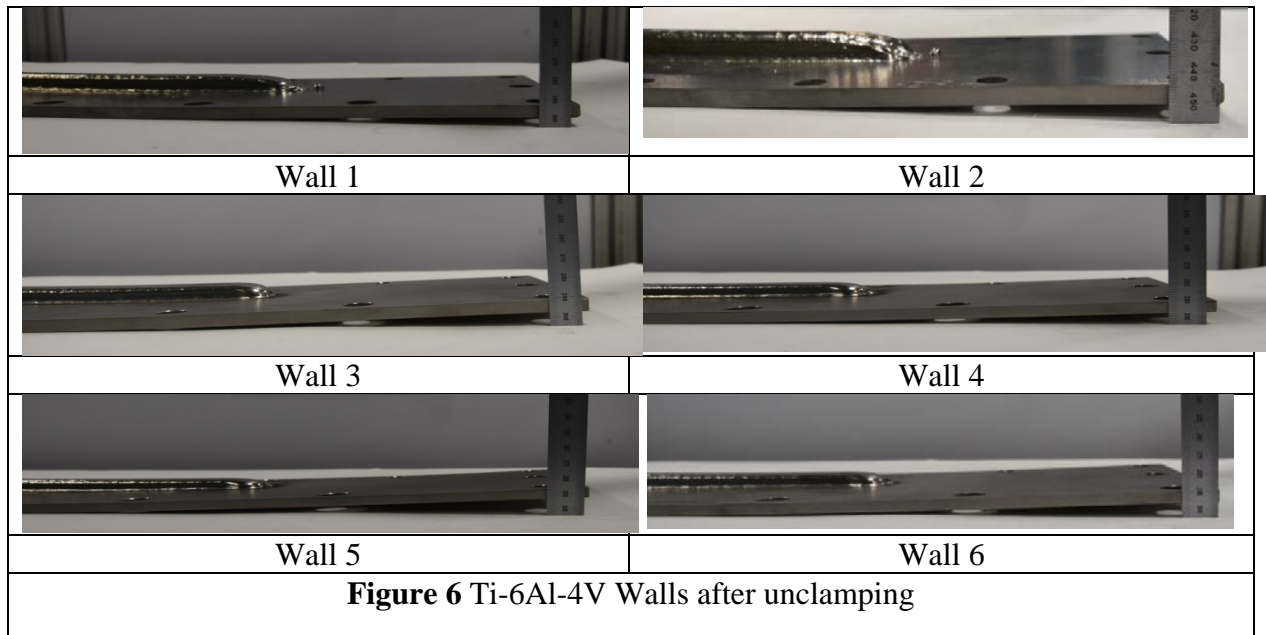


Table 4 Vertical deformation of un-clamped deposited walls

| Sample ID | Vertical deformation (mm) |
|-----------|---------------------------|
| Wall 1 | 6 |
| Wall 2 | 7 |
| Wall 3 | 8 |
| Wall 4 | 7 |
| Wall 5 | 12 |
| Wall 6 | 9 |

All six deposited walls were used to extract samples for room temperature tensile testing in accordance with the ASTM E-08 13a standard. One half of the wall was tested in an as-deposited condition, while the other half was subjected to the heat treatment recommended by the AMS 4999 standard, which involved annealing the samples at 538 °C +/- 14 for 4 hours +/- 0.25. Table 4 compares the monotonic tensile properties of as-deposited samples across different processing conditions, while Table 5 compares the tensile properties of their heat-treated counterparts.

Table 5 Tensile properties of as-deposited samples

| Sample ID | Temp. | UTS (ksi) | 0.2 YS (ksi) | Elong (%) | Reduction in Area (%) | Modulus (Msi) |
|-----------|-------|-----------|--------------|-----------|-----------------------|---------------|
| Wall 1 | Room | 144.2 | 127.0 | 8.0 | 13 | 16.4 |
| Wall 2 | Room | 145.5 | 128.8 | 11 | 19 | 16.8 |
| Wall 3 | Room | 143.9 | 128.0 | 11 | 22 | 14.5 |
| Wall 4 | Room | 146.1 | 129.5 | 11 | 23 | 15.5 |
| Wall 5 | Room | 145.6 | 129.2 | 13 | 24 | 15.9 |
| Wall 5 | Room | 144.1 | 127.0 | 13 | 21 | 16.5 |

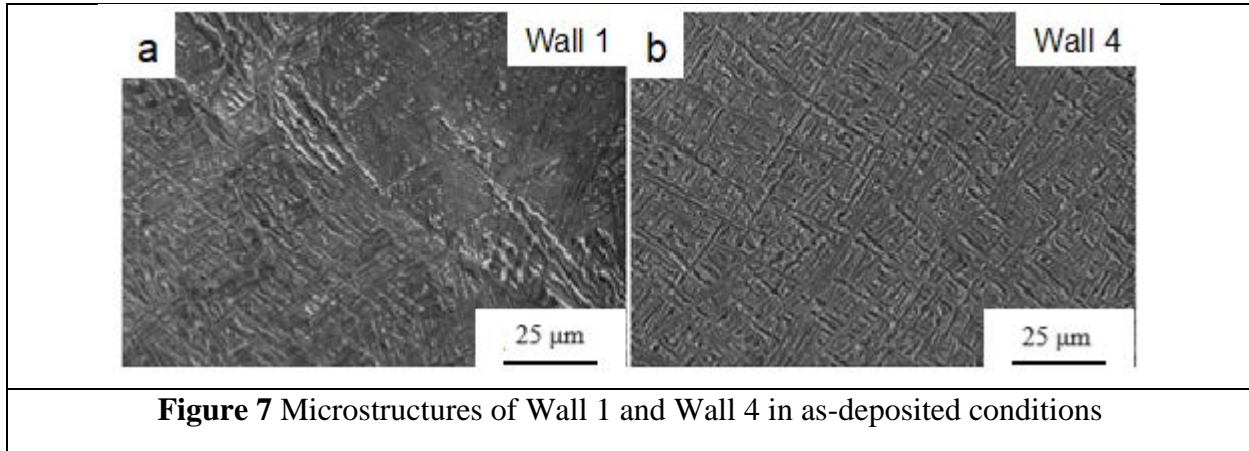
Table 6 Tensile properties of heat treated samples

| Sample ID | Temp. | UTS (ksi) | 0.3 YS (ksi) | Elong (%) | Reduction in Area (%) | Modulus (Msi) |
|---------------------|-------|-----------|--------------|-----------|-----------------------|---------------|
| Heat Treated Wall 1 | Room | 136.5 | 123.6 | 13 | 18 | 15.5 |
| Heat Treated Wall 2 | Room | 139.8 | 126.8 | 15 | 32 | 15.6 |
| Heat Treated Wall 3 | Room | 138.2 | 124.7 | 15 | 24 | 15.6 |
| Heat Treated Wall 4 | Room | 139.7 | 126.6 | 11 | 13 | 15.9 |
| Heat Treated Wall 5 | Room | 140.9 | 128.0 | 15 | 29 | 16.1 |
| Heat Treated Wall 5 | Room | 139.9 | 127.6 | 15 | 30 | 16.0 |

In the as-deposited condition, the samples have similar Yield Strength (YS) and ultimate tensile strength (UTS) irrespective of the processing condition involved. However, there is some scatter in the elongation to failure. The similarity of YS may arise from near similar microstructures in the as-deposited condition, whereas the scatter in elongation may result from the presence of porosity in the as-deposited samples. Upon heat treatment, there is a noticeable drop in the YS and UTS values in all cases, and yet again the properties are within scatter. There is an increase in elongation on the heat-treated samples in general. The reduction in strength along with the increase in elongation is indicative of microstructural coarsening that is to be expected at the annealing temperatures. To better understand the impact of varying cooling times and clamping states during deposition of these samples, the microstructures from two extreme cases (Wall 1 and Wall 4) were evaluated via scanning electron microscopy. The micrographs are presented in Figure 7.

Microscopic examination shows the presence of basketweave in both the processing conditions. However, the similarity in microstructures is intriguing. These similarities in microstructures may have been caused by the start plate, or heat sink, being much larger than the part itself. Thus, Wall 1 maintained a high enough cooling rate over 10 layers to result in a basketweave microstructure. However, in the case of Wall 4, the cooling rate was as fast as that of Wall 1 during the deposition of the first two layers. In such a case, the deposited bead may already have cooled down to the background substrate temperature, which acts as a heat sink. On deposition of the subsequent two layers after a 30 minutes wait, if the prior layers are already at the background temperature, then the cooling rate will be similar as the build progresses. Thus, in the limited 10-layer build, the effect of the larger heat sink dominates over any potential impact the inter-layer cooling time can have. However, for taller, it is very likely that a continuous build

may have a coarser microstructure compared to one that has substantial inter-layer cooling time because of the thermal buildup resulting from the poor thermal conductivity of titanium.



5. Conclusions and Future Work

- 1) Cooling time between deposited layers influences the distortion of the plate, and unclamped samples showed more distortion than the clamped samples.
- 2) Longer inter-layer cooling time will cause larger distortion.
- 3) Since the built walls were not high, all the heat was transferred to the large heat sink or start plate thus, similar microstructure and mechanical properties are seen.
- 4) Wall 1 showed minimal distortion. Thus, for building large scale parts that are 10 layers or less, it is recommended not to use any inter-layer cooling time. This way total production time can be reduced.
- 5) Cooling time influences distortion but not mechanical properties for large scale parts that are not high.
- 6) There is a need to correlate amount of distortion to microstructure and mechanical properties for large scale components.
- 7) There is also a need to focus on the deposition pulling away from the start plate due to the residual stress build up.

6. Acknowledgements

The research was sponsored by the US Department of Energy, Office of Energy Efficiency and Renewable Energy, Advanced Manufacturing Office under contract DE-AC05- 15 00OR22725 with UT-Battelle, LLC. This work is also supported in part by Cooperative Research and Development Agreement with GKN Aerospace, under contract No. NFE-15- 05725.

7. References

- [1] B. Dutta, V. Singh, H. Natu, J. Choi, and J. Mazumder, "Direct Metal Deposition," *Adv. Mater. Process*, vol. 167, no. 3, pp. 33–36, 2009.
- [2] M. Technologies, "Laser engineered net shaping process-optimization of surface and microstructures," *Met. Powder Rep.*, vol. 53, no. 9, p. 57, 1998.

- [3] G. Escobar-Palafox, R. Gault, and K. Ridgway, "Robotic manufacturing by shaped metal deposition: state of the art," *Ind. Robot An Int. J.*, vol. 38, no. 6, pp. 622–628, 2011.
- [4] W. Du, Q. Bai, and B. Zhang, "A Novel Method for Additive/Subtractive Hybrid Manufacturing of Metallic Parts," *Procedia Manuf.*, vol. 5, pp. 1018–1030, 2016.
- [5] K. Taminger and R. Hafley, "Electron beam freeform fabrication: a rapid metal deposition process," *Proc. 3rd Annu. Automot. Compos. Conf.*, pp. 9–10, 2003.
- [6] Y. Bandari, S. Williams, J. Ding, and F. Martina, "Additive Manufacture of Large Structures: Robotic or Cnc Systems," *26th Int. Solid Free. Fabr. Symp.*, pp. 17–25, 2015.
- [7] "Optimization of Weld Bead Geometry in Tig Welding Process Using Grey Relation Analysis and Taguchi Method," *Mater. Technol.*, vol. 43, no. 3, pp. 143–149, 2009.
- [8] S. W. Williams, F. Martina, A. C. Addison, J. Ding, G. Pardal, and P. Colegrove, "Wire+Arc Additive Manufacturing," *Mater. Sci. Technol.*, vol. 23, pp. 73–80, 2015.
- [9] F. Martina, J. Mehnen, S. W. Williams, P. Colegrove, and F. Wang, "Investigation of the benefits of plasma deposition for the additive layer manufacture of Ti–6Al–4V," *J. Mater. Process. Technol.*, vol. 212, no. 6, pp. 1377–1386, Jun. 2012.
- [10] Y. F. Hsiao, Y. S. Tarng, and W. J. Huang, "Optimization of Plasma Arc Welding Parameters by Using the Taguchi Method with the Grey Relational Analysis," *Mater. Manuf. Process.*, vol. 23, no. 1, pp. 51–58, 2007.
- [11] Sciaky, "Electron beam additive manufacturing," 2016.
- [12] W. U. H. Syed, A. J. Pinkerton, and L. Li, "A comparative study of wire feeding and powder feeding in direct diode laser deposition for rapid prototyping," *Appl. Surf. Sci.*, vol. 247, no. 1–4, pp. 268–276, 2005.
- [13] A. Heralić, "Monitoring and Control of Robotized Laser Metal-Wire Deposition," 2012.
- [14] E. R. Denlinger, J. C. Heigel, P. Michaleris, and T. A. Palmer, "Effect of inter-layer dwell time on distortion and residual stress in additive manufacturing of titanium and nickel alloys," *J. Mater. Process. Technol.*, vol. 215, pp. 123–131, 2015.
- [15] P. Michaleris and A. Debicari, "Prediction of welding distortion," *Am. Weld. Soc. - Weld. J.*, vol. 76, no. April, p. 172–s, 1997.
- [16] K. Masubuchi, *Analysis of Welded Structures : Residual Stresses , Distortion , and Their Consequences (International Series on Materials Science and Technology)*. Pergamon Press.
- [17] M. V. Deo and P. Michaleris, "Mitigation of welding induced buckling distortion using transient thermal tensioning," *Sci. Technol. Weld. Join.*, vol. 8, no. 1, pp. 49–54, 2003.
- [18] N. W. Klingbeil, J. L. Beuth, R. K. Chin, and C. H. Amon, "Residual stress-induced warping in direct metal solid freeform fabrication," *Int. J. Mech. Sci.*, vol. 44, no. 1, pp. 57–77, 2002.
- [19] D. Corbin, A. R. Nassar, E. (Ted) Reutzler, A. M. Beese, and P. (Pan) Michaleris, "Effect Of Substrate Thickness And Preheating On The Distortion Of Laser Deposited Ti-6Al-4V," *J. Manuf. Sci. Eng.*, vol. 140, no. June, 2018.
- [20] A. H. Nickel, D. M. Barnett, and F. B. Prinz, "Thermal stresses and deposition patterns in layered manufacturing," *Mater. Sci. Eng. A*, vol. 317, no. 1–2, pp. 59–64, 2001.
- [21] J. Fessler, R. Merz, A. Nickel, F. Prinz, and L. Weiss, "Laser deposition of metals for shape deposition manufacturing," *Solid Free. Fabr. Symp. Proceedings, Univ. Texas Austin*, pp. 117–124, 1996.
- [22] L. Costa, R. Vilar, T. Reti, and A. M. Deus, "Rapid tooling by laser powder deposition: Process simulation using finite element analysis," *Acta Mater.*, vol. 53, no. 14, pp. 3987–

- 3999, 2005.
- [23] B. Torries, S. Shao, N. Shamsaei, and S. Thompson, "Effect of Inter-Layer Time Interval on the Mechanical Behavior of Direct Laser Deposited Ti-6Al-4V," *Solid Free. Fabr. Proc.*, pp. 1272–1282, 2016.
 - [24] A. Lundbäck, "Modelling and Simulation of Welding and Metal Deposition," 2010.
 - [25] A. Plati, J. C. Tan, I. O. Golosnoy, R. Persoons, K. Van Acker, and T. W. Clyne, "Residual stress generation during laser cladding of steel with a particulate metal matrix composite," *Adv. Eng. Mater.*, vol. 8, no. 7, pp. 619–624, 2006.
 - [26] J. Grum and M. Žnidaršič, "Microstructure and residual stress analysis after laser cladding of low-carbon steel with powdery SiC, stellite 6, and stellundum 481," *Mater. Sci. Forum*, vol. 426–432, no. 3, pp. 2521–2526, 2003.
 - [27] V. Ocelík, J. Bosgra, and J. T. M. de Hosson, "In-situ strain observation in high power laser cladding," *Surf. Coatings Technol.*, vol. 203, no. 20–21, pp. 3189–3196, 2009.
 - [28] J. Ding, P. Colegrove, J. Mehnen, S. Williams, F. Wang, and P. S. Almeida, "A computationally efficient finite element model of wire and arc additive manufacture," *Int. J. Adv. Manuf. Technol.*, vol. 70, no. 1–4, pp. 227–236, Jan. 2014.
 - [29] J. Ding, "Thermo-mechanical Analysis of Wire and Arc Additive Manufacturing Process," no. January, p. 216, 2012.
 - [30] J. L. Prado-Cerqueira, J. L. Diéguez, and A. M. Camacho, "Preliminary development of a Wire and Arc Additive Manufacturing system (WAAM)," *Procedia Manuf.*, vol. 13, pp. 895–902, 2017.
 - [31] F. Montevocchi, G. Venturini, N. Grossi, A. Scippa, and G. Campatelli, "Idle time selection for wire-arc additive manufacturing: A finite element-based technique," *Addit. Manuf.*, vol. 21, no. December 2017, pp. 479–486, 2018.
 - [32] S. Simunovic, A. Nycz, M. W. Noakes, C. Chin, and V. Oancea, "Metal Big Area Additive Manufacturing : Process Modeling and Validation," June, pp. 1–17, 2017.